Cryogenics 146 (2025) 104002

Contents lists available at ScienceDirect

Cryogenics

journal homepage: www.elsevier.com/locate/cryogenics

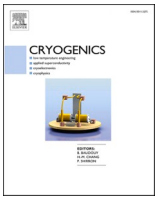

Residual resistance ratio measurement system for Nb_3Sn wires extracted from Rutherford cables

Ian Pong [a,*], Algirdas Baskys [b,c], Charlie Sanabria [b,d], Michael Naus [a], Scott Myers [a], Heng Pan [b,e], Jonathan Lee [b,f], Li Wang [a], Jordan Taylor [b], Marcos Turqueti [a], Xiaorong Wang [a]

[a] Lawrence Berkeley National Laboratory, Berkeley, CA 94720, USA
[b] Formerly with Lawrence Berkeley National Laboratory, Berkeley, CA 94720, USA
[c] Now with CERN, Geneva 1211, Switzerland
[d] Now with Commonwealth Fusion Systems, Cambridge, MA 02139, USA
[e] Now with Chengdu Finsiot Inc., No. 1366, Middle Tianfu Ave., Wuhou District, Chengdu, China
[f] Now with the Applied Superconductivity Center, National High Magnetic Field Laboratory, Tallahassee, FL 32310, USA

ARTICLE INFO

Keywords:
Superconductors
Residual resistance ratio
Nb_3Sn
Cryocooler
Cryogen-free

ABSTRACT

Residual resistance ratio (RRR) of superconducting strands is an important parameter for magnet electrical stability. RRR serves as a measure of the low-temperature electrical conductivity of the copper within a conductor that has a copper stabilization matrix. For Nb_3Sn, due to the need of a reaction heat treatment, the technical requirements for high quality measurements of strands extracted from Rutherford cables are particularly demanding. Quality of wire, cabling deformation, heat treatment temperature, heat treatment atmosphere, sample handling, and measurement methods can all affect the RRR. Therefore, as an integral part of the electrical quality control (QC) of Nb_3Sn Rutherford cables manufactured at the Lawrence Berkeley National Laboratory, it was prudent that we established a RRR measurement system that can isolate the assessment of cable-fabrication-related impacts from sample preparation and measurement factors.

Here we describe a bespoke cryocooler-based measurement system, capable of measuring RRR of over 80 samples in a single cooldown. The samples are mounted on custom-designed printed circuit boards that accommodate the shape of strands extracted from a Rutherford cable without added deformation, which we will show is critical in ensuring that the measurements accurately represent the RRR values of the conductor within the cable. Using this sample mounting solution, we routinely measure the overall RRR of the strand as well as individual intra-strand sections corresponding to both cable edges and cable broad faces with high reproducibility. Such measurements provide valuable information on the variation of RRR along the length of the strands as well as across strand productions and cable runs over time.

1. Introduction

High critical current density, or high-J_C, Nb_3Sn conductors are liable to experience magneto-thermal instabilities at low magnetic fields leading to flux jumps [1]. This may be a problem if it leads to premature magnet quenches while ramping the magnet current. The propensity for flux jumps depends on a variety of parameters, including critical current (I_C), strand diameter, effective filament size, and the RRR of the stabilizing copper [2,3]. The high-J_C Nb_3Sn wires for accelerator magnet applications typically have a distributed diffusion barrier design with a large effective filament size, such as the RRP® design made by Bruker OST. RRR for Nb_3Sn is defined in the IEC 61788–4 standard [4] as the ratio of conductor resistance at 293 K to its resistance just above the superconducting transition, T_C:

$$RRR = R_{293K}/R_{T_c} \quad (1)$$

RRR measurements on wires are often made by a direct current (D. C.) 4-point technique on a holder attached to the end of a probe that is inserted into a liquid helium dewar, lowered slowly down the temperature gradient until the sample is superconducting, and then raised slowly back above T_C. Alternatively, the samples may be placed in a dedicated cryostat in which liquid helium is transferred and allowed to

* Corresponding author.
E-mail address: ipong@lbl.gov (I. Pong).

https://doi.org/10.1016/j.cryogenics.2024.104002
Received 11 October 2024; Received in revised form 2 December 2024; Accepted 5 December 2024
Available online 9 December 2024

slowly vapourise for the temperature to rise gradually. The samples may be a short straight sample with a voltage tap distance of a few mm [5] or a small coil about a metre long [6], and the holder may have a flat backing plate with a cover [7], a pair of cylindrical half shells [8], or may be free standing [9].

Studies have shown that RRR values below ~ 100 [1–3] have an increasingly deleterious effect on the stability of conductor stands, either standalone or as incorporated in cables and coils in accelerator magnets. Nb_3Sn conductor needs a heat treatment to form the superconducting phase, during which time Sn can diffuse into the stabilizing Cu, causing an increase of the residual resistance, thus degrading the conductor's RRR value. It is often the case that the strand and cable designs and the heat treatment parameters require a balancing act between RRR, J_C and the irreversible strain limit [10]. For example, the High Luminosity upgrade of the Large Hadron Collider Accelerator Upgrade Project (HL-LHC AUP) adopted a strand design that has a slightly reduced Sn content in order to boost the RRR at the expense of only a marginal reduction of critical current [11]. Experiments have also shown that the critical current of Rutherford cables can be well estimated by that of individual extracted strands, and the RRP® strand type has a predictable ~ 5 % J_C degradation, thus allowing extracted strand I_C to be routinely used for quality control (QC) in lieu of the more expensive whole-cable I_C measurements [12]. However, despite limited I_C reduction, if RRR degradation is significant, reduction of the stability current, I_S, may pose a performance issue [13]. Therefore, RRR measurements on extracted strands are integral to the electrical quality control (QC) of Nb_3Sn Rutherford cables.

When measuring the RRR of the wires extracted from Rutherford cables, it is important to consider the non-uniform deformation along the wire length [14]. During Rutherford cable fabrication, the strands experience significantly greater plastic deformations at the cable edges, where the strands transition from one broad face layer to the other, than on the broad faces. Moreover, if the cable has a non-zero keystone angle, across its width the thickness is not identical, with one side more compacted and deformed (minor edge) than the other (major edge). At the cable edges (where individual strands are "kinked"), the subelements within the wire exhibit the most severe shape distortions [15]. The subelement distortions increase the chance of thinning or rupture of the diffusion barriers, resulting in the Sn in the subelement diffusing past the barrier (i.e. leaking) into the Cu stabilizer. Even in minute amounts below standard chemical detection limits, Sn leaks can "poison" the high purity Cu to cause a noticeable increase in the amount of lattice scattering and electrical residual resistance at cryogenic temperatures, thus significant suppressing the RRR [16]. When the Sn leak is only at the cable edge, the severity of local degradation of RRR may not be correctly assessed by a RRR measurement over the entire length of an extracted strand that includes both the kinked and straight sections. For this reason, we have chosen to measure the four characteristic segments in each extracted strand individually: the kinked major and minor edges, and the straight sections along the top and bottom faces of the Rutherford cable (see Fig. 1).

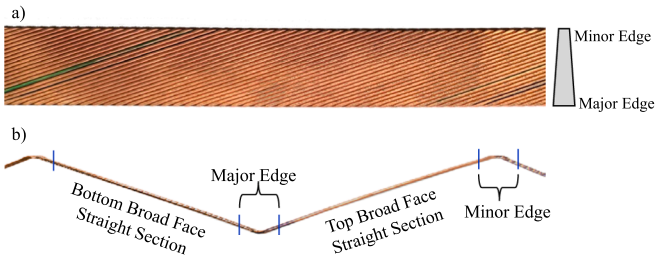

Fig. 1. A) an example of a 40-strand Rutherford cable manufactured for the HL-LHC AUP project [17]. Two strands near the ends of the cable are colour-coded to aid individual strand identification for QC purposes. b) A Nb_3Sn strand segment extracted from a cable. Four segments of the strand, corresponding to the bottom broad face, major edge, top broad face, and minor edge are measured individually, and are labeled in the figure above.

Given the short voltage tap distance needed to measure the local resistance at the cable edges, a highly reproducible process is necessary. For this reason, we investigated the effects of different aspects of sample preparation and measurement methodology. In this paper, we report how our approach to preserve the deformation state of the strands after the extraction from a Rutherford cable can yield RRR values representative of the local status of the strands within a Rutherford cable.

2. System design

The following subsections show an overview of the system, including the mechanical, vacuum, cryogenic, and electrical components, as well as the temperature control, measurement, and data acquisition and interpretation.

2.1. Mechanical, vacuum and cryogenic components

The system comprises a large, outer stainless steel vacuum vessel / cryostat "shell" supported by an aluminium extrusion frame and an inner aluminium "can" that thermally shields a copper sample board carrier (see Fig. 2). The top of the cryostat ("RT (room temperature) top plate"), which also supports the cryocooler and contains two KF-50 and six KF-40 ports for the vacuum valves and electrical feed-throughs, is rigidly fixed to the aluminium frame. The stainless steel shell below is made from a ¼" thick sheet formed into a cylinder, welded together, and then welded to the top and bottom flanges made from ¾" thick plates. This shell can be lowered to expose the inner aluminium can and the copper sample holder. This outer stainless steel vacuum shell, which weighs over 50 kg, is constrained laterally by a set of roller guides that slot into the aluminium extrusion, whereas the vertical movement is facilitated by a manual forklift.

The vacuum seal between the bottom of the RT top plate and the top flange of the stainless steel shell is achieved by a rubber O-ring, and the seal can be conveniently broken and re-made via a set of eight swivel bolts on clevis pins and nuts on the upper flange. The vacuum seal between the bottom plate and the stainless steel shell is also achieved by a rubber O-ring, but the seal is more permanently made via a set of 12 cap screws on the lower flange. The interior of the cryostat is evacuated before operation using a Pfeiffer HiCube 80 Classic vacuum pump. Pressure within the cryostat during operation is in the range of 2–5 x 10^{-7} mBar.

The inner aluminium thermal radiation shield, which has a 38 cm inner diameter and weighs only about 5 kg, hangs from an aluminium plate ("intermediate temperature plate"). This shield hangs via six threaded studs on its flange that can be manually inserted through six keyhole slots on the intermediate temperature plate. Standard nuts on the threaded studs fit through the eyes of the slots and the shield is then rotated to be hung in place (where the narrow portions of the slots catch the nuts). There is no O-ring needed at this interface, since the volume on either side of the aluminium "can" is under the same vacuum. The interface here is a rough polished aluminium-to-aluminium flat surface which is sufficient for good heat transfer to thermally anchor the aluminium shell to the cryocooler's 1st stage. In our present setup, no multilayer insulation is necessary between the stainless steel shell and the aluminium can. The intermediate temperature plate is mechanically suspended from the room temperature top plate by four carbon fiber straps (to accommodate lateral thermal contraction while limiting thermal conduction). The intermediate temperature plate in turn supports the copper sample holder assembly (Fig. 3) by four stainless steel threaded rods.

The samples are conduction cooled using a Cryomech PT415 cryocooler (compressor model CP1010), with cooling capacity of 1.5 W at 4.2 K and 40 W at 45 K. The first stage of the cryocooler is thermally linked to the aluminium thermal radiation shield around the samples via

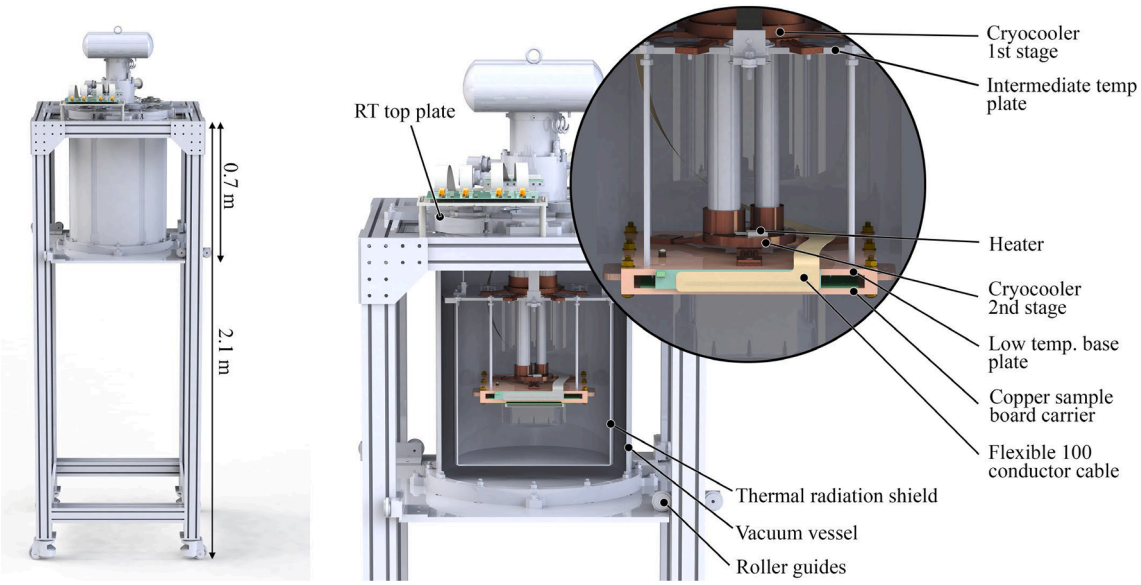

Fig. 2. Overview of the residual resistance ratio measurement system. The top flange of the cryostat with the cryocooler is stationary, while the stainless steel vacuum vessel (or "shell") as well as the aluminium thermal shield (a.k.a. "can") can be lowered, providing access to the sample holder fixture for sample exchange.

the intermediate temperature plate. During operation, the first stage temperature typically gets as low as 36–38 K. The second stage of the cryocooler is thermally connected to a low temperature base plate and in turn to the copper sample holder assembly via braided copper cables with indium foils at the interface. The copper sample holder assembly reaches an ultimate temperature of around 4–6 K.

Sample temperature control is achieved via two heaters attached to the second stage of the cryocooler (the front heater can be seen in Fig. 2 as indicated; the back heater is behind it on the opposite end also on the top side of the second stage). The heater power and cryocooler first and second stage temperatures are monitored by a Lakeshore 331 cryogenic temperature controller, while the sample temperature is read by a Lakeshore 218 temperature monitor. All temperatures are measured using calibrated Lakeshore Cernox® sensors, with the exception of an optional backup verification temperature sensor, which uses a calibrated Lakeshore PT-102-AL sensor that operates down to ~ 30 K.

An example temperature cycle is shown in Fig. 4 and a flowchart of our standard operation procedure for AUP extracted strands with an accelerated warmup is shown in Fig. 5. It typically takes approximately 10 h to cool down and stabilize the system. When the sample carrier is at the base temperature and the wire samples are superconducting, measurements can begin. In this example temperature profile, the warmup half-cycle was not accelerated, i.e. the chamber vacuum is maintained, and the stage heaters were not switched on. The heat leak into the system warms up the PCB and the second stage by less than 6 K h^{-1} at a steady rate from liquid nitrogen temperatures to room temperature, comparable to the heater-controlled warm up rate of lower temperatures (see section 2.4). This translates to about 1.6 mK per second, which can allow this system to be used during natural warmup for low temperature physics experiments in this temperature range, such as critical temperature measurements of high temperature superconductors, with excellent accuracy. Using the accelerated warmup procedure (see section 2.4), the system can reach room temperature in about one-fifth the time.

2.2. Sample holder assembly

The combination of a large cryostat and adaptable sample holder assembly allows a large number of samples to be accommodated for measurements. Samples are affixed to custom printed circuit boards (PCB) up to approximately 25 cm x 20 cm. A typical board for straight wire can accommodate 45 samples of 10 cm length in two columns, whereas a typical board for extracted strands can accommodate a total of 18 samples (see Fig. 3). A thick ¼" copper base plate with two edge rails (a.k.a. side spacers) encasing the samples increases temperature uniformity, and the construction allows multiple assemblies to be stacked vertically.

Strands extracted from a Rutherford cable have a sawtooth shape, whose width and pitch length differ between cable designs. For measured RRR of extracted wires to be representative of those in the cable, extracted wire samples should not be straightened (see section 4.1 for justification). To assure repeatability and to minimize handling, we build custom PCBs with voltage tap placement according to each unique cable design to tailor to the sample shape. The samples are held in place by Y-shaped slot pins acting as voltage taps (Fig. 3**a inset**). Only the slots at the ends of the sample that provide the test current are soldered to the sample. The voltage taps are typically reliably held in contact by friction and by the elasticity of the slots without requiring the aid of an additional electrically conducting medium. This greatly simplifies the mounting and de-mounting of samples.

The voltage tap spacing is selected to separate the straight sections of the extracted strand that form the top and bottom broad faces of the cable and the kinked segments that are the cable edges. The characteristic segment lengths vary by cable design. As an example, for HL-LHC AUP extracted strands, the voltage taps at the cable edges are 10 mm apart. This covers the ~ 3 mm long part where the strand transitions from the top layer to the bottom layer (or vice versa) containing the facet which is the most heavily deformed portion of the extracted strand, and symmetrically another ~ 3 mm on each side that form the "triplet" of the cable edge [15]. Wire segments at the cable edge have higher subelement deformation and thus typically lower RRR and critical current. A greater voltage tap distance would "dilute" the RRR degradation, and it is critical for a highly reproducible system to avoid having to manually solder voltage taps onto the samples.

Our alternative design for straight samples utilizes screw-tightened terminal blocks for mounting (Fig. 3**b inset**). Here, care must be taken to avoid excessive force when tightening the screws. The advantage of such a mounting mechanism is that the sample board can be attached directly to the low temperature base plate with samples facing down. In addition to the samples, each board typically contains connections for up to two thermometers.

In our experience, we found that thinner PCBs without backing metallic coatings are easier to work with. Thick PCBs, especially ones

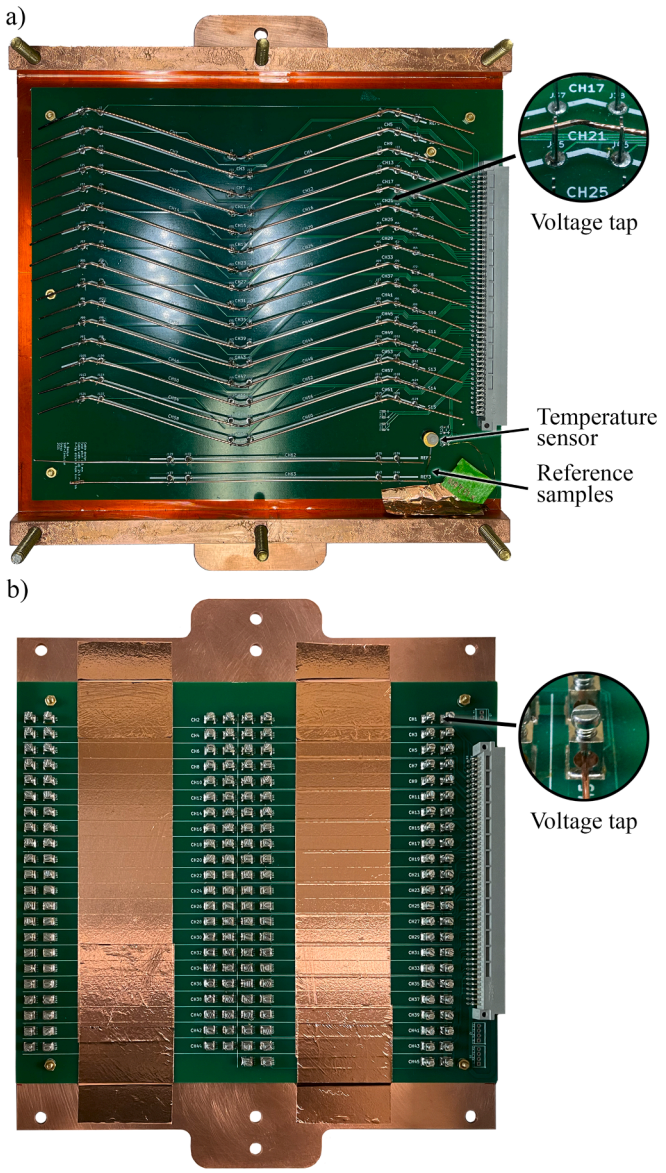

Fig. 3. A) An extracted sample holder with a PCB for samples extracted from cables manufactured for the Test Facility Dipole [18]. The arrows point to two straight reference samples and the location of a Cernox® thermometer. b) A sample board capable of measuring 45 straight samples during a single cool-down. Both PCBs are attached to a copper carrier base that bolts to a low temperature base plate which is thermally linked to the second stage of the cryocooler but mechanically suspended from the intermediate temperature plate. PCBs with size up to 25x20 cm can be accommodated.

with multiple trace layers are more prone to warping during cooldown, thus adversely compromising the thermal transfer such that even with an indium layer between the PCB and the copper carrier, the samples may not be able to achieve a low enough temperature to see superconducting transitions. Backing metallic coatings are unfriendly to through holes on PCBs (such as those for mounting the Y-shaped pins) and can too easily cause electrical shorts. They may also contribute to thermal warping.

2.3. Electrical design

At present, the system is configured for up to 120 channels split between two independent sample boards, but can be further extended easily. The signals from the sample board are carried to the outside of

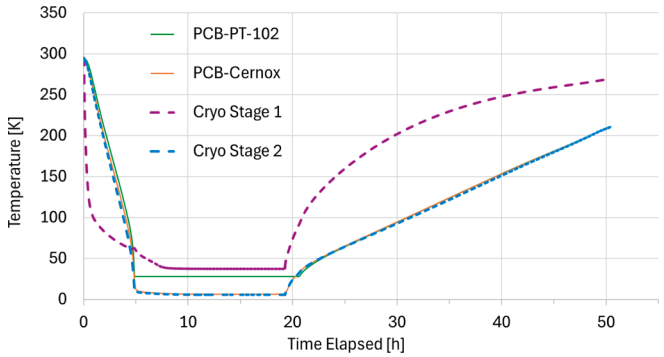

Fig. 4. An example temperature cycle. The warm up half-cycle was without acceleration, i.e. helium gas was not let into the chamber and vacuum was maintained, and the heaters remained off. The Cryo-stage temperature sensors are mounted on the intermediate temperature plate and the low temperature base plate.

the cryostat via two 100-conductor ribbon cables (23 mm wide 1.8 m long, see Fig. 6) manufactured as a 2-layer custom circuit board with polyimide as the substrate and 0.1 mm wire traces. (The total copper conductor cross-sectional area is 0.35 mm^2 per cable.) This was chosen to reduce the heat-leak to the sample board without the need to thermally intercept the cable at the 1st stage of the cryocooler. The ribbon cable exits the cryostat through a slot in a blank ISO-KF 40 flange sealed by "Torr Seal" low vapor pressure epoxy. Outside of the cryostat the signals are distributed to the DB78 connectors, which carry the signals to the Keithley 3706A system switch equipped with two Keithley 3724 multiplexer cards with 60 channels each. The voltage measurements are performed with a Keithley 2182A nanovoltmeter. The excitation current, typically of ± 0.5 A, is provided by a Yokogawa GS610 Source Measure Unit (Fig. 7).

The wires carrying the excitation current are separate from the ribbon carrying the signals, so that they can be of larger diameter and be thermally intercepted at the 1st and 2nd cryocooler stages. The wiring for the excitation current and thermometers that are not mounted to the sample board are taken outside the cryostat using a circular multi-pin feedthrough on a KF 40 flange.

2.4. Measurement control and data acquisition

Measurement is controlled via a custom LabView program. The measurement closely follows the IEC 61788–4 standard on the measurement of RRR of Nb-Ti and Nb_3Sn composite superconductors [4] and the LBNL system has been qualified and benchmarked with other facilities [19]. Below is a description of our standard operating procedure for a 0.85 mm diameter HL-LHC AUP strand.

After evacuating the cryostat and cooling down to base temperature, a current is applied to the samples. The current is modified according to the sample diameter if necessary to avoid excessive self-heating (< 1 A/mm^2, typically 0.5 A). The excitation current polarity is reversed between every measurement in order to eliminate any offsets due to thermal EMFs in the system. This is particularly important because the signal path contains multiple junctions at different temperatures across the system, and the temperature is ramped during the measurement. The temperature is ramped at a rate of approximately 0.1 K/min to 20 K (past the superconductive-normal transition, which is typically near 18 K for Nb_3Sn) using PID control of the 2nd stage heaters. At this point the cryocooler is switched off and the samples are allowed to return to room temperature. To accelerate the process, a small amount of helium gas is allowed into the vacuum chamber (1–2 mBar). The warm-up can be further accelerated by enabling the 2nd stage heater. Data is continually collected as the samples warm up past 293 K. With a fully populated HL-LHC AUP extracted strands PCB of 63 voltage taps, the

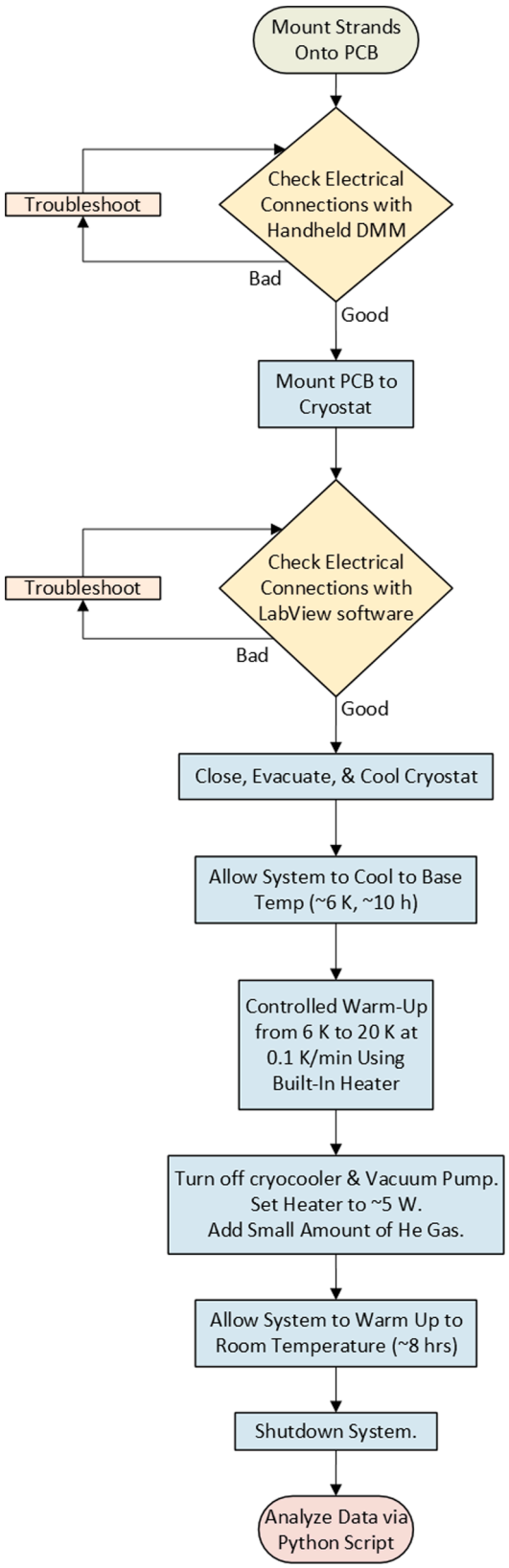

Fig. 5. A high-level flow chart showing our standard operation procedure for AUP extracted strands. Note: DMM = digital multimeter.

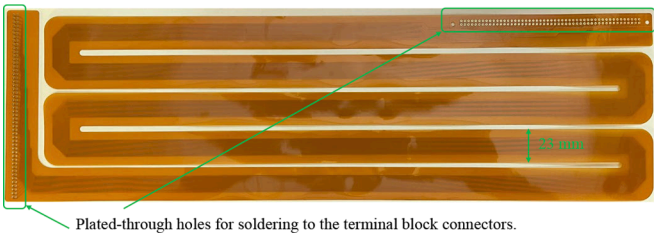

Fig. 6. A flexible 100-conductor, 23 mm wide ribbon cable for taking measured signals outside the cryostat while keeping the thermal leak into the cryostat to a minimum. The cable is manufactured folded (or zigzag, as shown above) to achieve the required length without exceeding the size limitations of the printed circuit board manufacturer and to minimize cost. The straight end of the cable exits the cryostat through a slit in a KF-40 blank (sealed with epoxy) mounted at one of the six KF-40 ports on the room temperature top plate. The right-angled end is for connecting to the sample PCB as seen in Fig. 2 via the grey connector on the right-hand side of each PCB show in Fig. 3.

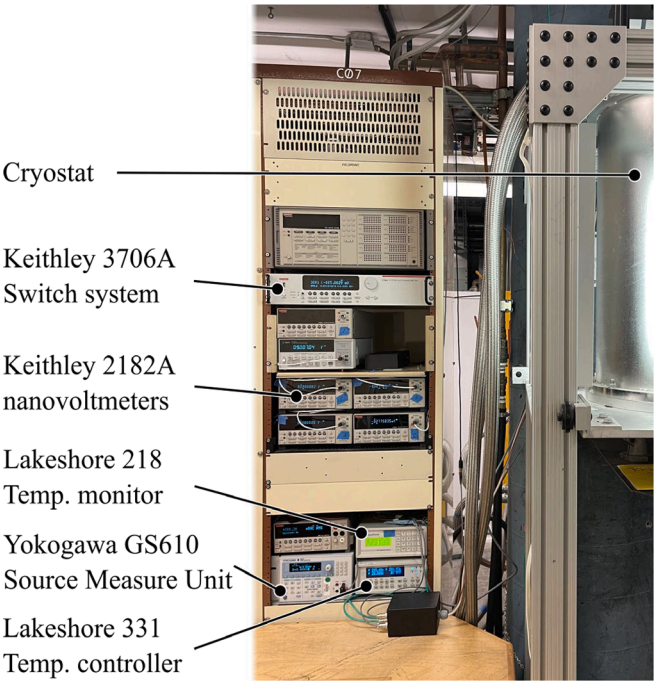

Fig. 7. Measurement system rack and the equipment used for the measurement (annotated). The cryostat and the cryostat stand are visible on the right.

sampling rate at each channel is every 5.2 s on average, translating to an achievable nominal temperature step of the order of ~ 0.01 K.

2.5. *Measurement data analysis*

Measurement data analysis is automated by a custom Python script. At low temperature, it creates linear fits to the data in the superconducting and normal states, and also of the transition. It then calculates the low temperature resistance by the intersection of the transition and the resistive fit lines (Fig. 8). The room temperature resistance value is taken as the sample warms up past the temperature of 293 K.

An advantage of using the superconductive transition instead of a specific temperature is that it removes the need for measuring the temperature of each sample individually near 20 K, when there may be slight differences in temperature from sample to sample across the board and away from the temperature sensor(s). Nevertheless, an effort is made to minimize the thermal gradient across the samples. On the other hand, this measurement method relying on the superconductive

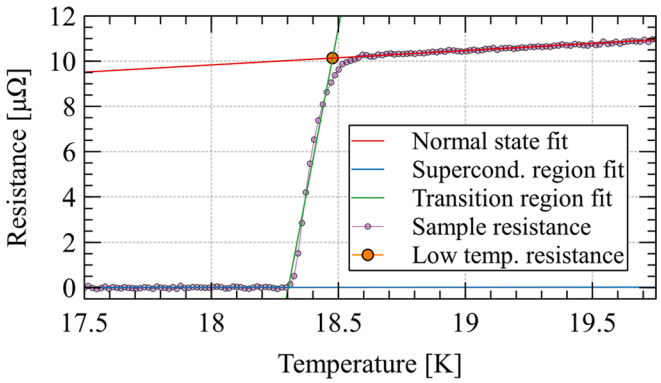

Fig. 8. An example curve of a sample resistance dependence on temperature near the superconducting transition. Resistance data for each sample is collected from 4 K to 293 K. The resistance at low temperature (R_{T_c} in equation (1) is taken as the orange dot in the plot.

transition requires resistance values to be taken across a larger temperature range (across the transition, not only a single temperature), as well as adds the need for post-measurement analysis.

3. Sample preparation and measurement reproducibility

To ensure integrity in the sample preparation and measurement, in addition to the candidate samples (e.g. 15 extracted strands in the case of US HL-LHC AUP per PCB cooldown), each measurement contains three additional "reference" samples. Each of the additional specimens has a specific function. Reference Sample #1 is a previously measured sample used as a check on the RRR measurement system; Reference Sample #2 is a witness sample to validate the heat treatment schedule; Reference Sample #3 is another witness sample to validate the atmosphere in the furnace during the heat treatment.

Reference Sample #1, a.k.a. RRR system reference, is a previously measured extracted strand that stays on the sample measurement board and does not get removed between measurements. If the RRR measurement system is functioning correctly, a consistent RRR value should be measured each time. Fig. 9 shows the measured RRR value of this reference sample as a function of time since the year 2021. The initial value spread was significantly improved by changes in data acquisition and automated analysis (see Section 2.5 above) since the end of 2021. As part of the upgrades, the old sample board was replaced, and as seen in the data, desoldering, removal and remounting of the sample resulted in slight decrease (4 units, ~1%) in the measured RRR value, likely due to deformation while handling the reference sample. The improved mounting board and automated analysis gives a remarkably reproducible consistency, as can be seen in Fig. 9.

Reference Samples #2 & #3 are heat treatment witnesses. The two

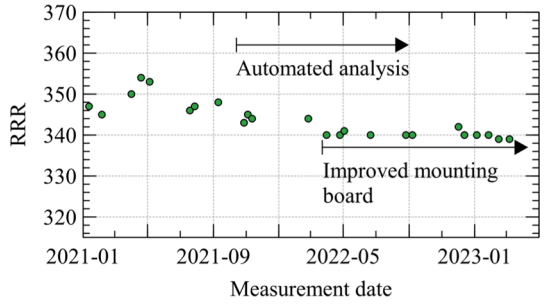

Fig. 9. RRR values of the reference sample measured on the system as a function of time. Automated analysis of data reduced the spread of determined RRR values. Handling the sample while moving it to a new sample mounting board resulted in a small but measurable RRR decrease.

samples are in straight, undeformed form and taken from a "reference spool" – the same, well characterized, wire spool for each measurement. These samples are used to validate the reaction heat treatment for the formation of Nb_3Sn, which is performed in a furnace under flowing argon atmosphere. Reference Sample #2 is encapsulated in a quartz ampoule with a piece of Ti wire as an oxygen getter. This sample will experience (or "witness") the same heat treatment temperature and duration as the candidate samples, but not the atmosphere. Reference Sample #3 is simply loaded into the furnace in the same state as the extracted strands, and as such, is not in a quartz tube. It will witness the heat treatment temperature and duration, as well as the atmosphere. In the case that the measured RRR value for either witness sample deviates from the values previously measured for the same spool, the integrity of heat treatment procedure would be more closely examined, and the candidate samples might be discarded. If both witness reference samples show a shift of the measured RRR values in the same direction, the likelihood is an incorrect heat treatment schedule (such as caused by an incorrectly calibrated temperature controller thermocouple). If only the non-encapsulated sample shows a deviation, the likelihood is a furnace atmosphere contamination (such as due to an air-leak) because such an event would not affect the encapsulated sample. All candidate samples measured in a cooldown are typically reacted in the same heat treatment as the two witness reference samples mounted on the same board.

The use of RRR system reference and heat treatment witness reference samples is our standard quality assurance procedure. It has proved to be invaluable when troubleshooting unexpected RRR values by helping identify potential problem sources. Furthermore, the witness reference samples have also provided a baseline of reliability and reproducibility of our heat treatment and sample preparation procedure. Their RRR values over more than two years since the end of 2021 in 14 different heat treatment runs achieved a single-digit standard deviation, comparing very favourably to international benchmarking exercises for internal tin strands such as reported in [20].

4. Effects of sample preparation and measurement methodology

Although RRR is a commonly used quality control parameter for superconducting wires, there are some variations in the measurement procedure that may result in slightly different values in the reported RRR. Some of these differences and their effect on the measurement result are explored in the following subsections.

4.1. Straightened and non-straightened extracted strand RRR

At other laboratories, strands extracted from Rutherford cables are often straightened before heat treatment to simplify the sample mounting fixture for RRR measurement. However, this carries the risk of further damaging subelements within the Nb_3Sn strand, making the values artificially lower than what they are in a Rutherford cable. Also, by doing so and taking one measurement over a length covering both straight sections and kinks, one loses information about the impact of deformation in the kinked sections of the cable in comparison to the straight (top and bottom cable face) segments. Straightening of the wire is not an easily controlled process and it is difficult to ensure such a procedure's reproducibility. The process would not only lower the overall RRR of the sample, but also preferentially decrease the RRR of the kinked edge segments. To quantify the effect of straightening the extracted strands, we tested 20 pairs of samples in an experiment. Each pair was extracted from the same strand within a Rutherford cable and from adjacent strand sections. Altogether, 20 pairs from 4 cables were used. One strand from each pair was straightened before heat treatment. The straightened strands were heat-treated in 2 mm internal diameter, open-ended quartz tubes to maintain the straightened shape after heat treatment. These and the non-straightened strands were wrapped together in an S-glass fiber cloth to space out the samples and prevent them from fusing together at high temperature, as is typically done for

our extracted strand heat treatment procedure. Both samples from each pair were reacted at the same time in the same furnace, and subsequently their RRR was measured. Any differences in the measured RRR values beyond experimental uncertainty would be attributable to the straightening procedure.

The results are shown in Fig. 10. The figure illustrates that RRR values in the straight segments and the cable edges are noticeably different, with cable edges having lower values of RRR as expected. Comparing the extracted strands that were straightened before heat treatment and those that were kept in their original shape, there is an observable reduction in the overall values, on average 5.3 %. However, the kinks that have experienced the most deformation during cable fabrication and during straightening show a somewhat larger reduction in RRR compared to non-straightened wires (on average 8.2 % lower at the minor edge). This degradation is attributed to further ruptures of the diffusion barriers at the kink, causing more extensive Sn contamination to the stabilization Cu.

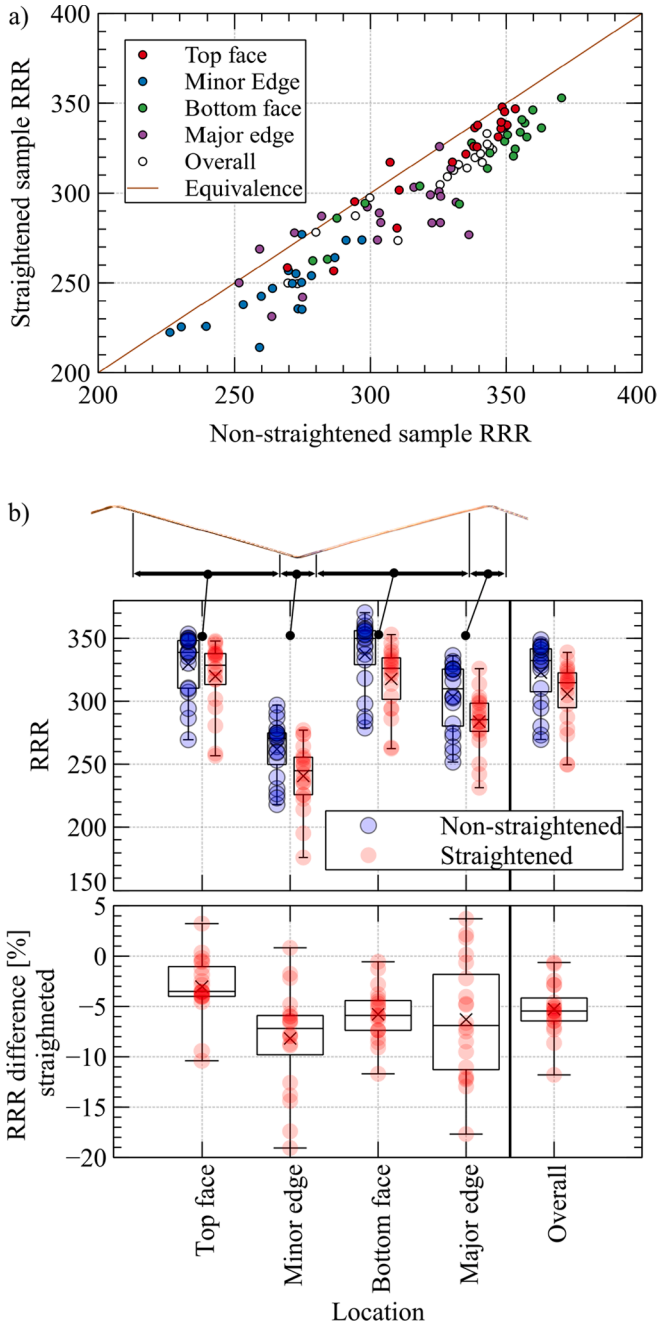

Fig. 10. A) Straightened sample RRR as a function of non-straightened sample RRR for each measured sample pair (20 pairs from 4 cables). b) Aggregate statistics – the top panel shows the RRR values plotted as a function of their location along the sample as indicated in the diagram above. The bottom panel shows the percent difference of RRR values of the samples taken from the same strands of the cable but straightened before heat treatment. The mean values are indicated by the cross, the whiskers indicate minimum and maximum values.

4.2. RRR at 20 K in comparison to RRR at T_C

It is not uncommon for RRR measurements of Nb_3Sn wires to measure the low temperature resistivity at a fixed temperature (often 20 K) instead of at the superconductive-normal transition. This can make the measurement easier, as the resistivity can be measured at a single temperature instead of across a range of temperatures near critical temperature T_C and the subsequent curve analysis is not needed. However, if many samples are measured simultaneously, there is a risk that a temperature gradient among the samples and the thermometer would impart an undesirable error to the measured RRR values.

Fig. 11 shows a plot of RRR at several temperatures as a function of RRR at T_C. The dashed lines are calculated using copper resistivity dependance on temperature for several RRR values using data in [21]. The datapoints in red show measured data for both round wires and strands extracted from Rutherford cables for three different RRP® wire designs with distinct Cu:non-Cu ratios (0.88 to 1.24), showing that the resistivity behavior of the Nb_3Sn wires is dominated by the stabilization copper.

As the samples are not in direct contact with the thermometer, there is a small temperature offset among them. That offset was calculated by considering the measured temperature at the critical temperature of each sample, taken to be 18.4 K. The validity of this approach was later confirmed by attaching the thermometer directly to a set of selected samples.

The data, as well as calculated curves, show a good match between RRR values measured near T_C and at 20 K up to about RRR ~ 100, the values then diverge and the RRR of 500 measured at 20 K is about 10 % lower than the corresponding value measured at T_C (500 vs. 550).

4.3. Dependence on the test current

Finally, the magnitude of the test current may influence the critical temperature and the resulting RRR at the critical current. A sample was tested with varying test currents, the results show only a slight dependence of T_C with varying test current in the range of 0.1 to 0.7 A. And the resulting RRR varies by less than 2 units for a sample with RRR of 338.3

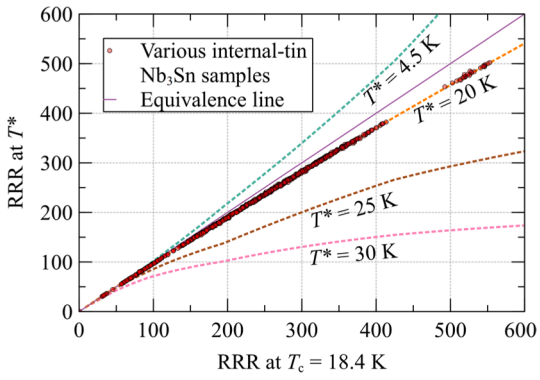

Fig. 11. Comparison of RRR defined with low temperature resistance measurement at Nb_3Sn T_C = 18.4 K and low temperature measurement at another temperature T^*. The dashed lines are data calculated for copper from [21]. The datapoints show values for various Nb_3Sn samples of RRP® design with Cu:non-Cu ratios spanning values from 0.88 to 1.24.

at 0.5 A test current. This implies that even with limited cooling due to poor thermal contact, sample handling is likely expected to introduce more variation than the choice of test current in the range investigated (see Fig. 12).

5. Lessons learned and future improvements

5.1. Thermal coupling of samples to cryocooler

Unsurprisingly, thermal coupling of samples to the second stage turned out to be the most challenging issue, due to the requirement of keeping the samples electrically insulated from the rest of the system. Printed circuit boards based on FR4 substrate are easy to work with, but their low thermal conductivity has resulted in some observed temperature differences among samples of up to 1 K at low temperatures. Although more thermometers may be placed in the vicinity of the samples to improve individual temperature reading accuracy, and although this temperature value is not relied upon in our RRR calculation (resistance value at T_C is used, rather than at a specific temperature), having better temperature uniformity can make our system more versatile. To improve temperature uniformity across the samples, aluminium substrate-based circuit boards are being tested, which should improve thermal conductivity by several orders of magnitude compared to FR4.

Thermal conduction between the samples and the copper base plate is typically sufficient through the voltage and current contacts. During system development, copper rails with disposable Kapton lining were used to sandwich the sample ends to provide additional thermal linkage to the copper sample holder assembly, but subsequent improvements to the thermal contact between the PCB and the copper base plate have removed that need. The removal of this step is advantageous because the Kapton lining can be punctured or compromised by the samples during loading or due to differential thermal contraction of various components, causing electrical shorts that may only be detected at cold and are thus time consuming to troubleshoot.

5.2. Sample fixturing and voltage taps

Sample mounting using Y shaped slot pins without needing to solder each individual voltage tap was shown to be reliable and can drastically reduce sample mounting and de-mounting effort. Moreover, given the narrow profile of the slot pins, they provide a well-defined voltage tap position. Initial trials also used a nylon ring on each voltage tap that would press the Y-slot more securely on the wire upon cooling (due to a larger Nylon thermal contraction, see Fig. 13). However, it was subsequently determined that good electrical contact with the pins was made even without the assistance from nylon rings. Similarly, carbon paste was initially used as a non-permanent electrical contact enhancer. However, due to its semiconducting behavior at cryogenic temperatures, the carbon paste introduced measurement errors and was not used in subsequent routine measurements.

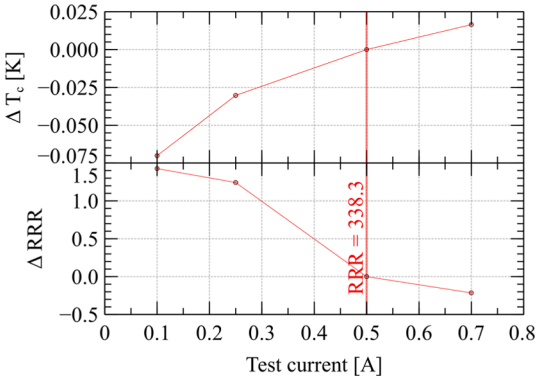

Fig. 12. Change in critical temperature and RRR as a function of test current used. The variations shown in the y-axis are compared to the current typically used, which is 0.5 A.

5.3. Measurement speed

Improvement of measurement speed by utilizing two or more nanovoltmeters for measuring two samples simultaneously is being considered. Such configuration is allowed by the switch system and could potentially allow for faster temperature ramp rates while maintaining data resolution in terms of temperature.

6. Summary

The system described above is designed as a versatile tool for measuring resistance ratio, and it is specifically tailored for efficient and reproducible measurements of both superconducting wires in straight form as well as extracted strands from Rutherford cables without straightening them first. The system allows the measurement of many samples in a single cooldown (currently configured for up to two sample boards that can carry up to 45 straight samples each, or a lower number of extracted cable strand samples with multiple voltage taps on each sample) and makes use of ribbon cables (flexible 2-layer, 100-channel custom circuit board with polyimide as the substrate) for taking measured signals outside the cryostat while keeping the thermal leak into the cryostat to a minimum.

In terms of operation procedures, we found the use of cooldown reference and heat treatment witness reference samples for Nb_3Sn invaluable to ensuring sample preparation quality. We further showed the straightening process often applied to strands extracted from Rutherford cables and that taking one measurement over a length without giving due distinction to the straight sections and the kinked cable edges make the measured RRR data less precise and accurate, and therefore less informative for cable quality assessment.

We also showed that in wires of different designs there is a good match between RRR values measured near T_C and at 20 K up to about RRR ~ 100, but the two then diverge and the RRR of 500 measured at 20 K is about 10 % lower than the corresponding value measured at T_C. Lastly, we found that even with restricted thermal contact, sample handling likely introduces more variation than a reasonable range of test currents would.

CRediT authorship contribution statement

Ian Pong: Writing – review & editing, Validation, Supervision, Software, Resources, Project administration, Methodology, Investigation, Funding acquisition, Formal analysis, Data curation, Conceptualization. **Algirdas Baskys:** Writing – review & editing, Writing – original draft, Software, Methodology, Formal analysis, Data curation. **Charlie Sanabria:** Validation, Methodology, Investigation, Data curation, Conceptualization. **Michael Naus:** Writing – review & editing, Methodology, Investigation, Formal analysis, Data curation. **Scott Myers:** Visualization, Validation, Conceptualization. **Heng Pan:** Software, Investigation. **Jonathan Lee:** Writing – review & editing, Software, Methodology, Investigation, Formal analysis, Conceptualization. **Li Wang:** Validation, Supervision, Investigation. **Jordan Taylor:** Software, Investigation, Conceptualization. **Marcos Turqueti:** Supervision, Methodology, Investigation, Conceptualization. **Xiaorong Wang:** Writing – review & editing, Methodology, Investigation, Conceptualization.

Declaration of competing interest

The authors declare that they have no known competing financial interests or personal relationships that could have appeared to influence

Fig. 13. Close up images of the (a) soldered current contact and (b) a typical pair of voltage taps at a cable edge. The dented face along the left-hand side of straight section is the inside face of the cable. (c) is an optional modification using a nylon ring to help secure the wire in the Y-slot.

the work reported in this paper.

Acknowledgements

The authors gratefully acknowledge the contributions of Tom Lipton and Adam Balough, who helped with the logistics and fixturing of the system, and of Edward Stafford, who helped with many standard AUP measurements. We also thank Giorgio Ambrosio, Lance Cooley, Dan Dietderich, Arup Ghosh, and Soren Prestemon for their leadership supporting the LARP Materials task at LBNL, during which phase we conceived and designed this system.

This manuscript has been authored by authors at Lawrence Berkeley National Laboratory under Contract No. DE-AC02-05CH11231 with the U.S. Department of Energy. The U.S. Government retains, and the publisher, by accepting the article for publication, acknowledges, that the U.S. Government retains a non-exclusive, paid-up, irrevocable, world-wide license to publish or reproduce the published form of this manuscript, or allow others to do so, for U.S. Government purposes.

Data availability

Data will be made available on request.

References

[1] Bordini B, Rossi L. Self Field Instability in High-Jc Nb_3Sn Strands With High Copper Residual Resistivity Ratio. IEEE Trans Appl Supercond 2009;19:2470–6. https://doi.org/10.1109/TASC.2009.2019086.

[2] Ghosh AK, Sperry EA, Cooley LD, Moodenbaugh AM, Sabatini RL, Wright JL. Dynamic stability threshold in high-performance internal-tin Nb_3Sn superconductors for high field magnets. Supercond Sci Technol 2005;18:L5–8. https://doi.org/10.1088/0953-2048/18/1/L02.

[3] Cooley LD, Chang PS, Ghosh AK. Magnetization, RRR and stability of Nb_3Sn strands with high sub-element number. IEEE Trans Appl Supercond 2007;17:2706–9. https://doi.org/10.1109/TASC.2007.898167.

[4] Superconductivity - Part 4: Residual resistance ratio measurement - Residual resistance ratio of Nb-Ti and Nb_3Sn composite superconductors. IEC 2020. https://webstore.iec.ch/publication/63789 (accessed June 14, 2023).

[5] Raine M. and Hampshire D. P., "Benchmarking of Nb_3Sn Strands". ITER Report in April, 2011. https://user.iter.org/?uid=2V2BEV.

[6] Godeke A., Bish P., Dietderich D.R., Gorham C.S., Hafalia A.R., Higley H.C., Liggins N.L., Mentink M.G.T. and Sabbi G.L., 2012, June. Novel methods for the measurement of the critical current of superconducting wires. In *AIP Conference Proceedings* (Vol. 1435, No. 1, pp. 209-216). American Institute of Physics. https://doi.org/10.1063/1.4712098.

[7] Cheggour N, Stauffer TC, Starch W, Goodrich LF, Splett JD. Implications of the strain irreversibility cliff on the fabrication of particle-accelerator magnets made of restacked-rod-process Nb3Sn wires. Sci Rep 2019 Apr 2;9(1):5466. https://doi.org/10.1038/s41598-019-41817-7.

[8] Lee KW, Kim KT. Fabrication of RRR Measuring System for Disseminating IEC International Standard. Progress in Superconductivity 2002;4(1):80–5.

[9] Charifoulline Z. Residual Resistivity Ratio (RRR) measurements of LHC superconducting NbTi cable strands. IEEE Trans Appl Supercond 2006;16:1188–91. https://doi.org/10.1109/TASC.2006.873322.

[10] Cheggour N, Stauffer TC, Starch W, Goodrich LF, Splett JD. Implications of the strain irreversibility cliff on the fabrication of particle-accelerator magnets made of restacked-rod-process Nb_3Sn wires. Sci Rep 2019;9:5466. https://doi.org/10.1038/s41598-019-41817-7.

[11] Cooley, L. D., et al. "Conductor specification and validation for high-luminosity LHC quadrupole magnets." *IEEE Transactions on Applied Superconductivity* 27.4 (2017) https://doi.org/10.1109/TASC.2017.2648738.

[12] Hopkins SC, Medina-Clavijo B, Rastoll C, Rodia D, Malabaila M, Barth C, et al. Deformation Behavior and Degradation on Rutherford Cabling of Nb_3Sn Wires. *IEEE Trans Appl Supercond* 2024;34(3). https://doi.org/10.1109/TASC.2024.3375274.

[13] Pong, Ian. "Processing of Low TC Conductors: The Compound Nb_3Sn." *Handbook of Superconductivity*. CRC Press, 2022. Pp. 213-275. ISBN: 9780429183027.

[14] Sumption MD, Nazareth V, Barzi E, Turrioni D, Yamada R, Zlobin A V., et al. Measurements Of RRR Variation in Strands Extracted from Nb_3Sn-Type Rutherford Cables. AIP Conf. Proc., vol. 986, AIP; 2008, p. 277–84. https://doi.org/10.1063/1.2900356.

[15] Baskys A, Croteau JF, Naus M, Perez C, Sanabria C, Lin A, et al. RRP Nb 3 Sn Subelement Shear Dependence on Hexagonal Subelement Stack Orientation and the Strand's Position Within a Rutherford Cable. *IEEE Trans Appl Supercond* 2023;33(5). https://doi.org/10.1109/TASC.2023.3265910.

[16] Brown M, Tarantini C, Starch W, Oates W, Lee PJ, Larbalestier DC. Correlation of filament distortion and RRR degradation in drawn and rolled PIT and RRP Nb_3Sn wires. Supercond Sci Technol 2016;29:084008. https://doi.org/10.1088/0953-2048/29/8/084008.

[17] Apollinari G, Carcagno R, Ambrosio G, Feher S, Ristori L. US contribution to the High Luminosity LHC Upgrade: Focusing quadrupoles and crab cavities. J Phys Conf Ser 2019;1350. https://doi.org/10.1088/1742-6596/1350/1/012005.

[18] Pong I, Hafalia A, Higley H, Lee E, Lin A, Naus M, et al. Cable Design and Development for the High-Temperature Superconductor Cable Test Facility Magnet. IEEE Trans Appl Supercond 2021;31. https://doi.org/10.1109/TASC.2021.3094410.

[19] Pong I, Sanabria C. AUP Superconductor QC Facility Qualification Report: LBNL Cryocooler RRR System Round Robin Samples Measurement Results 2018. https://us-hilumi-docdb.fnal.gov/cgi-bin/sso/ShowDocument?docid=1585 (accessed June 21, 2023).

[20] Pong, I., Jewell, M.C., Bordini, B., Oberli, L.R., Liu, S., Long, F., Boutboul, T., Readman, P., Park, S.H., Park, P.Y. and Pantsyrny, V., 2012. Worldwide Benchmarking of ITER Internal Tin Nb_3Sn and NbTi Strands Test Facilities. *IEEE transactions on applied superconductivity*, *22*(3), Art. No. 4802606. https://doi.org/10.1109/TASC.2012.2182972.

[21] Simon N, Drexler E, Reed R. Properties of copper and copper alloys at cryogenic temperatures. Final report 1992. https://doi.org/10.2172/5340308.